

Removal and mechanism of Ni(II)-containing wastewater by oxidation and Fe-impregnated modified biochar

Chaoyang Yu^{a,b}

^aCollege of Architecture and Environment, Sichuan University, Chengdu 610041, China, email: ran540301@163.com

^bSichuan-Tibet Railway Co., Ltd., Chengdu 610041, China

Received 27 September 2021; Accepted 3 February 2022

ABSTRACT

In this paper, raw biochar (RB), oxidation biochar (OB), and Fe-impregnated biochar (MB) were prepared and used to remove Ni(II) from aqueous solutions. Batch adsorption experiments showed that the Ni(II) removal efficiency by RB, OB, and MB could be guaranteed to reach 80%, 91%, and 99%, respectively, in the pH range of 5–10, indicating that the materials have strong pH adaptability. The coexisting ions Na⁺, Ca²⁺, and Fe³⁺ had little effect on the Ni(II) removal, while Cd²⁺ and Pb²⁺ had an inhibitory effect on the Ni(II) removal. The Ni(II) removal process was following the pseudo-second-order model and Langmuir model. The Ni(II) maximum adsorption capacity by RB, OB, and MB was 62.20, 80.25, and 110.60 mg/g at 298 K, respectively. The Ni(II) removal efficiency on MB was still able to reach 100% in different water bodies. After 5 adsorption–desorption experiments, the Ni(II) removal efficiency by RB, OB, and MB remained around 51%, 70%, and 90%, respectively. Notable, co-precipitation, ion-exchange, electrostatic interaction, and complexation may exist in the mechanism of Ni(II) removal by biochar. This study shows that impregnated treated biochar has the potential and prospect for better treatment of Ni(II)-containing wastewater.

Keywords: Biochar; Modified; Ni; Adsorption capacity; Mechanism

1. Introduction

With the rapid development of railroad construction in China's highlands, a large number of alloy sound insulation panels were used to be placed on both sides of the railroad to mitigate noise pollution generated by trains. Nickel is one of the essential materials for alloy materials. A large amount of Ni(II) wastewater was generated during the manufacturing process of sound insulation panels and caused serious pollution to the environment [1,2]. Ni-containing wastewater pollution posed a serious threat to human health and had attracted widespread attention from all walks of life at home and abroad [3–5]. Unlike other pollutants, heavy metal pollution was not only non-degradable but also enriching in the human body. Heavy

metal pollutants migrated and transformed through the food chain and concentrate in living organisms, thus indirectly entering the human body and seriously endangering human health [6,7]. Ni(II) was highly toxic and carcinogenic and can damage the brain, spinal cord, and internal organs of the human body, as well as poison aquatic organisms [8,9]. Therefore, it was necessary to deal with heavy metal pollution represented by Ni(II) pollution in wastewater.

Currently, there were several major methods for removing heavy metals from aqueous solutions, including chemical precipitation, ion-exchange, solvent extraction, ultrafiltration, reverse osmosis, electrodialysis, and adsorption [10–12]. However, most of these methods were unsustainable in developing countries due to high maintenance costs and several other factors (e.g., trace contaminants and large

amounts of precipitated sludge) [13]. The adsorption method was of great interest to domestic and foreign scholars because of its low cost, simple operation, high treatment efficiency, and lack of secondary contamination [14–18]. Biochar, which was obtained by oxygen-limited or anaerobic pyrolysis of agricultural and forestry wastes, was a green adsorbent that can successfully remove heavy metal ions from water [13,19,20]. However, the adsorption capacity of biochar in its pristine state may be low for heavy metals. Therefore, the pristine biochar may need further modification treatment to improve the adsorption performance [17,21]. Several modification methods had been used for the biochar modification, including alkali/acid treatment, steam activation, cationic modification, and impregnation [22,23]. Hu et al. [13] used Na_2S modification of corncob biochar to improve the specific surface area and pore volume of biochar, thereby enhancing the adsorption capacity of corncob biochar for Ni(II). The Ni(II) adsorption capacity by biochar increased from 20.38 to 35.50 mg/g by the co-modification of $\alpha\text{-Fe}_2\text{O}_3$ and $\alpha\text{-FeOOH}$ [24]. Therefore, a simple method to modify the performance of biochar and to improve its adsorption of heavy metal ions was necessary.

In this work, oxidation biochar (OB) and Fe-impregnated biochar (MB) were prepared by oxidizing and Fe-impregnating modified origin biochar and used for the Ni(II) removal from aqueous solution. The objectives were: (1) to improve the Ni(II) adsorption capacity by modifying biochar; (2) to evaluate the adsorption isotherms and kinetic studies; (3) to determine the interaction mechanism between Ni(II) and biochar; and (4) to provide a novel adsorbent for Ni-containing wastewater generated during the manufacture of alloy sound insulation panels.

2. Materials and methods

2.1. Reagents

Experimental reagents: $\text{FeCl}_3 \cdot 6\text{H}_2\text{O}$, $\text{FeSO}_4 \cdot 7\text{H}_2\text{O}$, H_2O_2 , $\text{NiSO}_4 \cdot 7\text{H}_2\text{O}$, concentrated hydrochloric acid, and concentrated sodium hydroxide. The reagents were all of the analytical reagent (AR) and were purchased from Sinopharm Reagent Group (Shanghai, China). The experimental water was deionized water (DW). Different concentrations of Ni(II) solutions were prepared by $\text{NiSO}_4 \cdot 7\text{H}_2\text{O}$.

2.2. Preparation of materials

2.2.1. Preparation of raw biochar

The deadwood was used as a relevant raw material to produce biochar. These camphor woods were collected from the campus of Sichuan University (Sichuan Province, China). The deadwood was repeatedly washed with deionized water until the adhering soil was removed. After air-drying for 7 d, the air-dried dead camphor wood was cut into wood segments of about 5 cm, and then a pulverizer was used to process the wood segments to produce powdered samples. Then the samples were put into a muffle furnace and flushed with N_2 as the protective gas. The temperature of muffle furnace was increased to 500°C at a rate of $5^\circ\text{C}/\text{min}$ and then kept for 2 h. After natural cooling, the biochar products were ground and passed through a 200 mesh sieve

and the sieved biochar was collected. The raw biochar (RB) sample was obtained and noted as RB.

2.2.2. Preparation of oxidized biochar [25]

Raw biochar (0.5 g) was mixed with 35 mL of H_2O_2 (5%) in a conical flask. Oxidation was carried out daily for 2–3 d in a constant temperature shaker at 80°C and 150 rpm. Then, the conical flask was transferred to a desiccator at 105°C and dried to constant weight. After drying, oxidized biochar samples were washed using DW. The oxidized biochar samples were obtained and noted as OB.

2.2.3. Preparation of Fe-impregnated biochar [26]

20 g of the original biochar was mixed with 200 mL of deionized water in a beaker. Then, the 20 g of $\text{FeCl}_3 \cdot 6\text{H}_2\text{O}$ and 11.1 g of $\text{FeSO}_4 \cdot 7\text{H}_2\text{O}$ were dissolved in 60 mL of deionized water in another beaker. The above two mixtures were mixed and stirred at 150 rpm for 30 min, and 1 mol/L NaOH was added dropwise to bring the pH of the solution to 11.0. The mixture was stirred for 2 h and then heated to a slight boil for 1 h and filtered, and the filtered solid was washed with DW to neutral. Then, the solid was dried in a constant temperature oven at 60°C for 12 h and stored. The resulting Fe-impregnated biochar was recorded as MB.

2.3. Adsorption experiments

2.3.1. Batch adsorption experiments

20 mg of the adsorbent was mixed with 50 mL, 10 mg/L of Ni(II) solution. The pH of the solution was adjusted by negligible 0.1 mol/L HCl or NaOH and subsequently placed in a constant temperature oscillator at 298 K and 150 rpm for 600 min to investigate the effect of coexisting ions (Ca^{2+} , Na^+ , Fe^{3+} , Pb^{2+} , and Cd^{2+}), the initial pH of the solution (2–10) and the strength of the background ion NaCl (0.001–0.1 mol/L) on the removal of Ni(II) by the adsorbent. After the reaction was completed, 10 mL of the solution was centrifuged for 10 min. Then the concentration of Ni(II) in the supernatant was determined by inductively coupled plasma emission spectrometry (Optima 7000 DV Model, ICP-OES). In addition, the release of cations (Na^+ and Ca^{2+}) from the solution was determined by ICP-OES. Finally, the removal efficiency [Eq. (1)] and the adsorption capacity [Eq. (2)] of Ni(II) were calculated.

$$R = \frac{C_0 - C_e}{C_0} \times 100\% \quad (1)$$

$$Q = \frac{(C_0 - C_e) \times V}{m} \quad (2)$$

where R is the removal efficiency of Ni(II), %; C_0 is the initial concentration of Ni(II), mg/L; C_e is the remaining concentration of Ni(II) in the solution after the adsorption equilibrium, mg/L; Q is the adsorption capacity, mg/g; V is the volume of the solution, mL; m is the mass of the adsorbent, mg.

2.3.2. Adsorption kinetics

The adsorption was carried out in a constant temperature oscillator at 298 K under the conditions of pH = 6, the dosage of 20 mg, and an initial concentration of 10 mg/L, respectively, to investigate the effect of reaction time (1–600 min) on the removal of Ni(II). To further understand the adsorption process, the pseudo-first-order model [Eq. (3)], pseudo-second-order model [Eq. (4)], and intraparticle diffusion model [Eq. (5)] were used for the fitting analysis, and the results are shown in Fig. 3 and Table 1.

$$q_t = q_e (1 - e^{-k_1 t}) \quad (3)$$

$$q_t = \frac{q_e^2 k_2 t}{1 + q_e k_2 t} \quad (4)$$

$$q_t = K_d t^{1/2} + C_i \quad (5)$$

where q_e and q_t are the adsorption capacity of Ni(II) by the adsorbent at the adsorption equilibrium and time “ t ”, respectively, mg/g; k_1 is the pseudo-first-order model, 1/min; k_2 is the pseudo-second-order model coefficient, g/(mg min); K_d is the intraparticle diffusion constant, mg/(m min^{1/2}); C_i is the boundary layer constant.

2.3.3. Adsorption isotherms

The effects of adsorption temperatures (288, 298, and 308 K) and initial concentrations (10–90 mg/L) on Ni(II) removal were investigated at pH = 6, the dosage of 20 mg, and an adsorption time of 600 min. The Langmuir model [Eq. (6)] and Freundlich model [Eq. (7)] were used for the fitting in this study.

$$q_e = \frac{q_{\max} K_b C_e}{1 + K_b C_e} \quad (6)$$

$$q_e = K_f C_e^{1/n} \quad (7)$$

where q_e is the adsorption capacity at equilibrium, mg/g; C_e is the concentration of Ni(II) at adsorption equilibrium; q_{\max} and K_b are the theoretical maximum adsorption capacity and Langmuir equilibrium constant, respectively; K_f and n are Freundlich equilibrium coefficient and dimensionless number, respectively.

To further understand the mechanism of Ni(II) removal by biochars, the experimental data were investigated by thermodynamic analysis. The Gibbs free energy change (ΔG°),

entropy change (ΔS°), and enthalpy change (ΔH°) were calculated by Eqs. (8) and (9).

$$\ln K^0 = \frac{\Delta S^\circ}{R} - \frac{\Delta H^\circ}{RT} \quad (8)$$

$$\Delta G^\circ = -RT \ln K^0 \quad (9)$$

where R is the gas constant (8.314 kJ/mol). K^0 is the equilibrium constant and T is the Kelvin temperature (K). The ΔG° , ΔH° , and ΔS° represent the standard free energy (kJ/mol), enthalpy (kJ/mol), and entropy (kJ/mol), respectively. The values of ΔH° and ΔS° were calculated from the slope and intercept of the linear regression curve of $\ln K^0$ vs. $1/T$ (Fig. 4d).

2.4. Characterization analysis

The adsorbent crystalline structure was analyzed by X-ray diffraction instrument (XRD, Bruker D8, Germany). The surface morphological features and elemental composition were analyzed by scanning electron microscopy with energy-dispersive X-ray spectroscopy (SEM-EDS, Zeiss SUPRA-40, Germany). The surface functional groups of the adsorbent were analyzed by Fourier-transform infrared spectroscopy (FTIR, Tensor 27, Germany). The specific surface area analysis of the biochar was analyzed by a specific surface area analyzer (BET, V-Sorb 2800TP, Chian). The surface potential changes of the biochar at different pH values were analyzed by a zeta potential analyzer, and the zero potential point was calculated.

2.5. Adsorption–desorption experiments

After adsorption of 10 mg/L of Ni(II) solution for 600 min at 298 K, pH 6.0, and dosage of 20 mg, the solution was filtered by centrifugation for 10 min. The reacted adsorbent was collected and desorbed by shaking in the addition of 1 mol/L NaOH solution for 12 h. The solid collected by centrifugation and filtration was dried in a constant temperature oven at 60°C for 12 h. The above experiments were repeated 5 times and the Ni(II) removal efficiency after each adsorption–desorption experiment was calculated.

3. Results and discussion

3.1. Characterization analysis

The SEM surface morphologies of biochars are shown in Fig. 1. As shown in Fig. 1a, the surface of RB was relatively smooth and had a small number of pores and blocky

Table 1
Fitting parameters for pseudo-first-order model and pseudo-second-order model

	Pseudo-first-order model				Pseudo-second-order model		
	$Q_{e,exp}$	$Q_{e,cal}$	k_1	R^2	$Q_{e,cal}$	k_2	R^2
RB	12.19	9.50	0.013	0.963	20.86	0.004	0.998
OB	16.82	8.85	0.020	0.989	22.89	0.007	0.999
MB	20.67	4.19	0.022	0.957	25.13	0.023	0.999

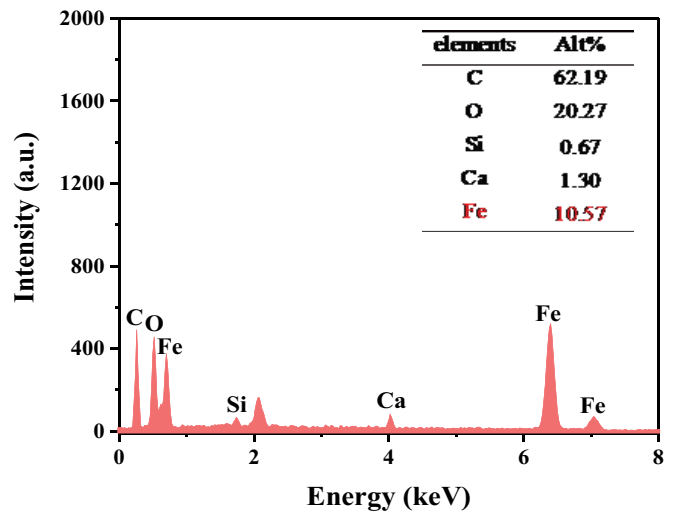
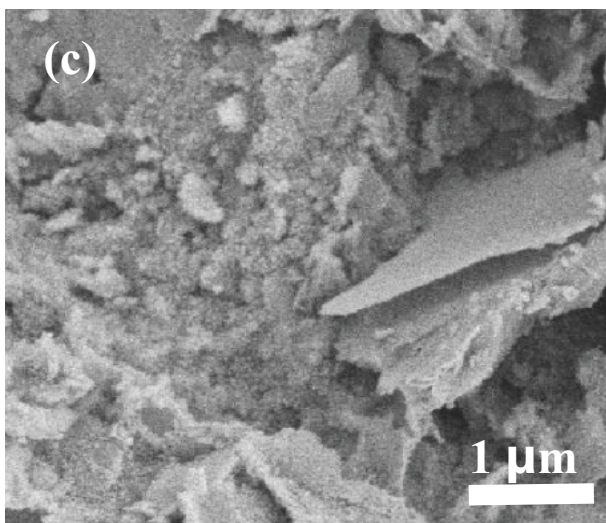
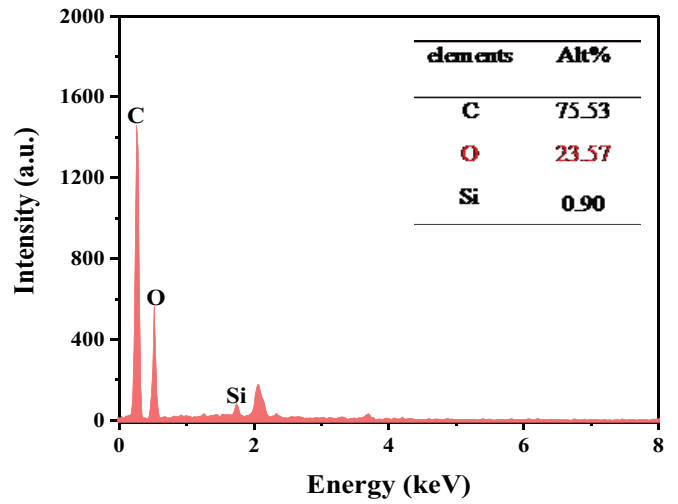
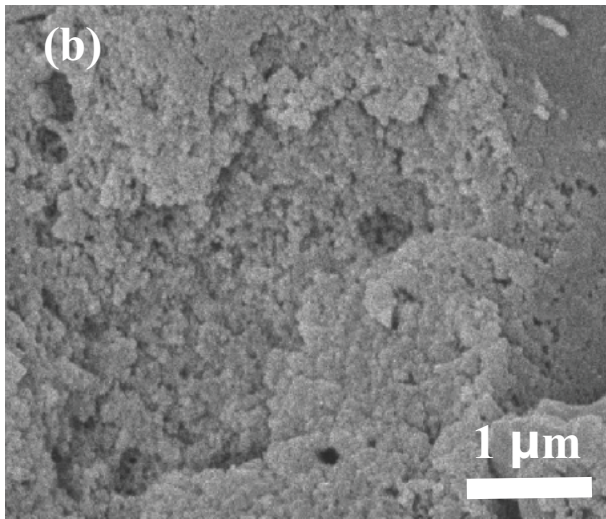
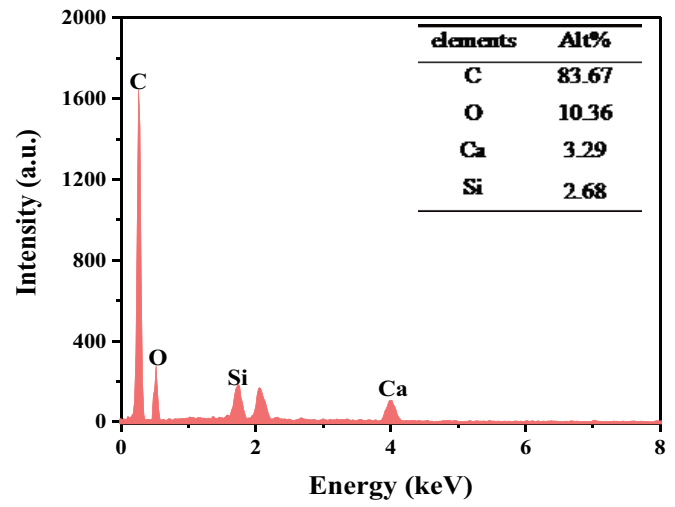
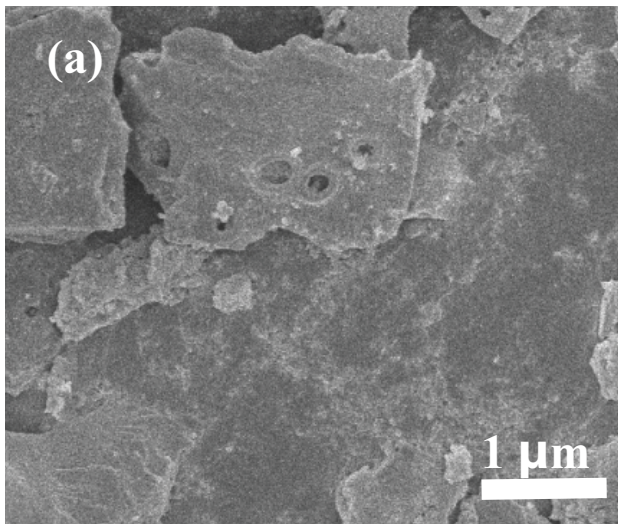
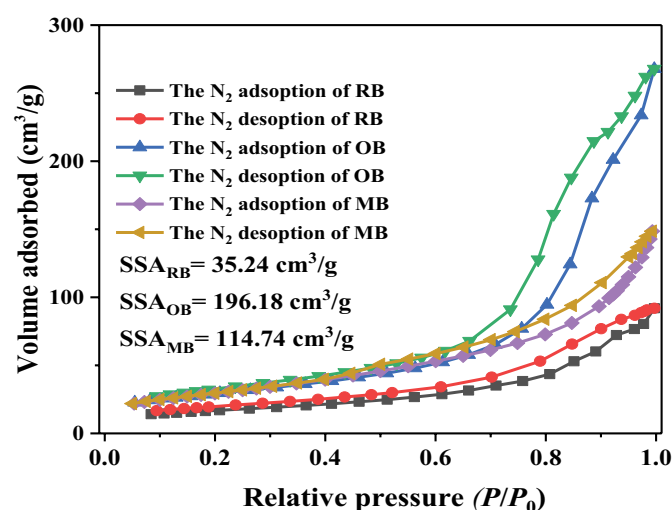


Fig. 1. SEM-EDS patterns of RB (a), OB (b), and MB (c).

distributed structures. In the morphology image of OR (Fig. 1b), the surface was rough and porous. Literature had been reported that the surface of biochar formed more pores and was uneven after oxidation [5,25]. As shown in Fig. 1c, the surface of MB was also rough and porous and had a lot of granular material uniformly distributed on the surface. In the EDS analysis, the O content in OB increased from 10.36% to 20.27% compared to RB, which indicated that the oxidation successfully increased the amount of O-containing functional groups in the biochar [25]. Notable, the MB contained 10.57% Fe, which indicated that the Fe element successfully covered the surface of the biochar. This also indicated that oxidation and impregnation were successful in preparing different types of biochar adsorbents.

The N_2 adsorption–desorption isotherm of the adsorbent is shown in Fig. 2a. As the relative pressure P/P_0 increased, the N_2 adsorption by the adsorbent gradually increased and a hysteresis loop was formed. This phenomenon indicated that the N_2 adsorption–desorption isotherm of the adsorbent can be classified as type IV isotherm and indicated that the adsorbent was a mesoporous material [8]. According to the calculation, the specific surface areas of RB, OB, and MB were 35.24, 196.18, and 114.74 cm^3/g , respectively. At a particular pH of the solution, the adsorbent dissociated into anions and cations to a comparable extent, and the solution was electrically neutral [3,27]. At this point, the solution pH was the zero potential point (pH_{pzc}) of the substance. The pH_{pzc} of the adsorbent is shown in Fig. 2b. The pH_{pzc} of RB, OB, and MB was 3.81, 2.88, and 4.26, respectively. When the solution pH was lower than pH_{pzc} , the H^+ in the solution occupied the O-containing functional groups on the adsorbent surface, which caused the O-containing functional groups on the adsorbent surface to be protonated and thus positively charged, and adsorbent was enhanced the adsorption capacity of anionic pollutants [14,28]. When the solution pH was higher than pH_{pzc} , the O-containing functional groups were deprotonated and turned to enhance the adsorption capacity of cationic pollutants [14].



3.2. Adsorption kinetics

As shown in Fig. 3, the Ni(II) adsorption capacity by the biochars first increased rapidly, and then slowly increased to the adsorption equilibrium. The faster adsorption stage was due to the presence of a large number of adsorption sites on the surface of the biochar [19,20]. However, with the increase of adsorption time the available adsorption sites decreased, which led to a slow increase of Ni(II) adsorption capacity by biochars [29]. Finally, adsorption reaction reached equilibrium. Notable, the equilibrium time for the Ni(II) adsorption by MB (60 min) was higher than that of OB (180 min) and RB (300 min).

By comparing the correlation coefficients R^2 of the pseudo-first-order model and pseudo-second-order model (Table 1), the pseudo-second-order model can better describe the adsorption process, suggesting that the adsorption process was chemisorption (e.g., ion-exchange or complexation) [10,30,31]. In addition, the theoretical adsorption capacity derived from the pseudo-second-order model was not much different from the actual adsorption capacity, which also indicated that the pseudo-second-order model can better describe the Ni(II) adsorption process by the biochars [6].

To further determine the reaction rate control process of the adsorbent on Ni(II), the kinetic data were fitted using the intraparticle diffusion model. The results of the fitting of the internal diffusion model for Ni(II) by biochar are shown in Fig. 3d, and the fitting parameters are given in Table S1. From Fig. 3d, the q_t showed a multilinear relationship for $t^{0.5}$, which indicated that the steps to control the adsorption rate were different at different stages of the adsorption process [32]. In the initial fast adsorption phase (Phase I), the Ni(II) diffused from the aqueous phase to the outer surface of the particle through an imaginary fluidic mesophase, which was the membrane diffusion stage [12,33]. In the fast adsorption phase, the adsorbent was able to contact more Ni(II). In addition, the Ni(II) concentration gradient at the interface between the liquid and solid phases was large. So, there was a high mass transfer

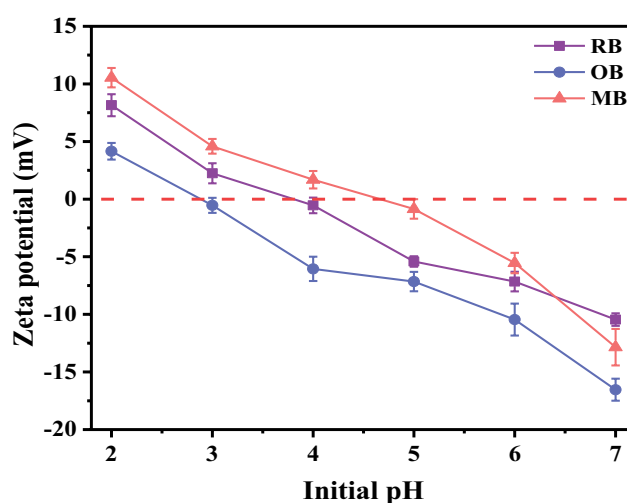


Fig. 2. N_2 adsorption–desorption and zero potential point (pH_{pzc}) of adsorbent.

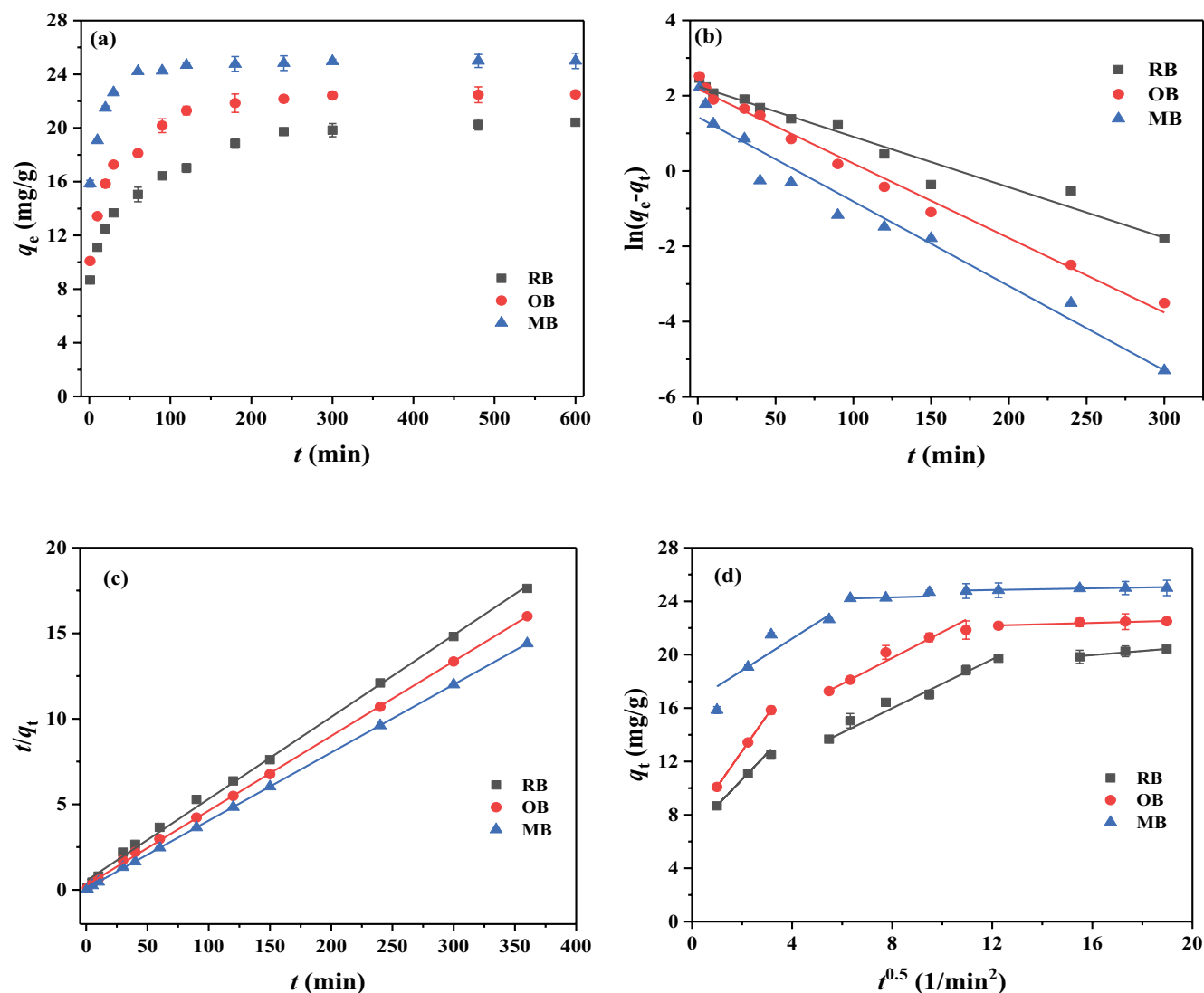


Fig. 3. Effect of time on the removal of Ni(II) by biochar (a), pseudo-first-order model (b), pseudo-second-order model (c) and intraparticle diffusion model (d) for Ni(II) removal by biochar.

driving force between the adsorbent and the adsorbent mass, which led to a relatively fast adsorption rate [28]. As the adsorption proceeded, Ni(II) entered the inner pore of the particle from the outer surface of the biochar and diffused it to the inner surface of the particle, which was the internal diffusion stage [9]. When the adsorption reaction proceeded to the second-stage, the adsorption sites on the adsorbent surface were gradually saturated. Then, Ni(II) was adsorbed to the inner surface inside the adsorbent, and the internal diffusion resistance increased continuously. With the decrease of Ni(II) concentration in the solution and the increase of internal diffusion resistance, the adsorption capacity slowly increased, and the adsorption reaction in this stage was the process of membrane diffusion and internal diffusion together [10]. At the later stage of adsorption, the Ni(II) concentration in the solution decreased a lot, and the adsorption process reached a steady state due to the increase of the internal diffusion resistance of the adsorbent and the saturation of the adsorption sites on the surface [15].

The Ni(II) adsorption kinetic behavior on biochars was following the pseudo-second-order model and the intraparticle diffusion model. It is further shown that the steps to control the adsorption rate in different stages of the adsorption process of biochar were different. Moreover, the Ni(II) adsorption by biochar was a chemical reaction.

3.3. Adsorption isotherm

As shown in Fig. 4a (RB), Fig. 4b (OR), and Fig. 4c (MB), the Ni(II) adsorption on biochar gradually increased and then tended to saturate. In addition, the Ni(II) adsorption capacity by the OR and MB was higher than that of the RB, indicating that the oxidation and Fe-impregnation successfully increased the Ni(II) adsorption capacity. The Ni(II) adsorption on the biochars increased with the increase of temperature, which suggested that the Ni(II) adsorption on the biochar was a heat absorption process [8,16].

The Langmuir model and the Freundlich model are shown in Fig. 4, and the parameters of the isotherm model are displayed in Table 2. The comparison of correlation coefficients ($R_1^2 > R_2^2$) suggested that the Langmuir model was more suitable to describe the process of Ni(II) removal by adsorbents, reflecting that the adsorption process was monolayer adsorption [15,32,34]. The Ni(II) adsorption capacities by RB, OB and MB were 62.20, 80.25, and 110.60 mg/g at 298 K. The large adsorption capacities were mainly due to the presence of a large number of O-containing functional groups on the surfaces of OB and MB, and Ni(II) could complex with O-containing functional groups ($-\text{COOH}$ and $-\text{OH}$) [25]. The K_b in Langmuir model can be used to illustrate the affinity between the adsorbent and Ni(II). The higher K_b value indicated that the adsorbent had a higher affinity for Ni(II) at the same temperature, which also suggested that the Ni(II) adsorption capacity of MB was higher than that of RB and OB [27]. Analysis of the reason for the larger adsorption capacity and affinity

of MB for Ni(II) may be related to its larger specific surface area and more O-containing functional groups, which can remove more Ni(II) from aqueous solution [35].

The thermodynamic parameters are shown in Table S2, and the enthalpy change ΔH° was positive, indicating that the Ni(II) adsorption process by the adsorbent was a heat absorption reaction. Moreover, the thermodynamic calculations were consistent with the experimental results depicted in Fig. 4a–c that the adsorption of Ni(II) by the adsorbent increased with increasing temperature. When the temperature increased from 288 K to 308 K, the ΔG° was all negative, suggesting that the Ni(II) adsorption by biochar was a spontaneous process [16]. The positive value of ΔS° indicated that the adsorption process of biochar on Ni(II) had an increased degree of freedom at its solid-liquid interface [14]. The results obtained for adsorption kinetics and adsorption isotherms indicated that the Ni(II) adsorption was dominated by chemisorption, such as ion-exchange and complexation [8].

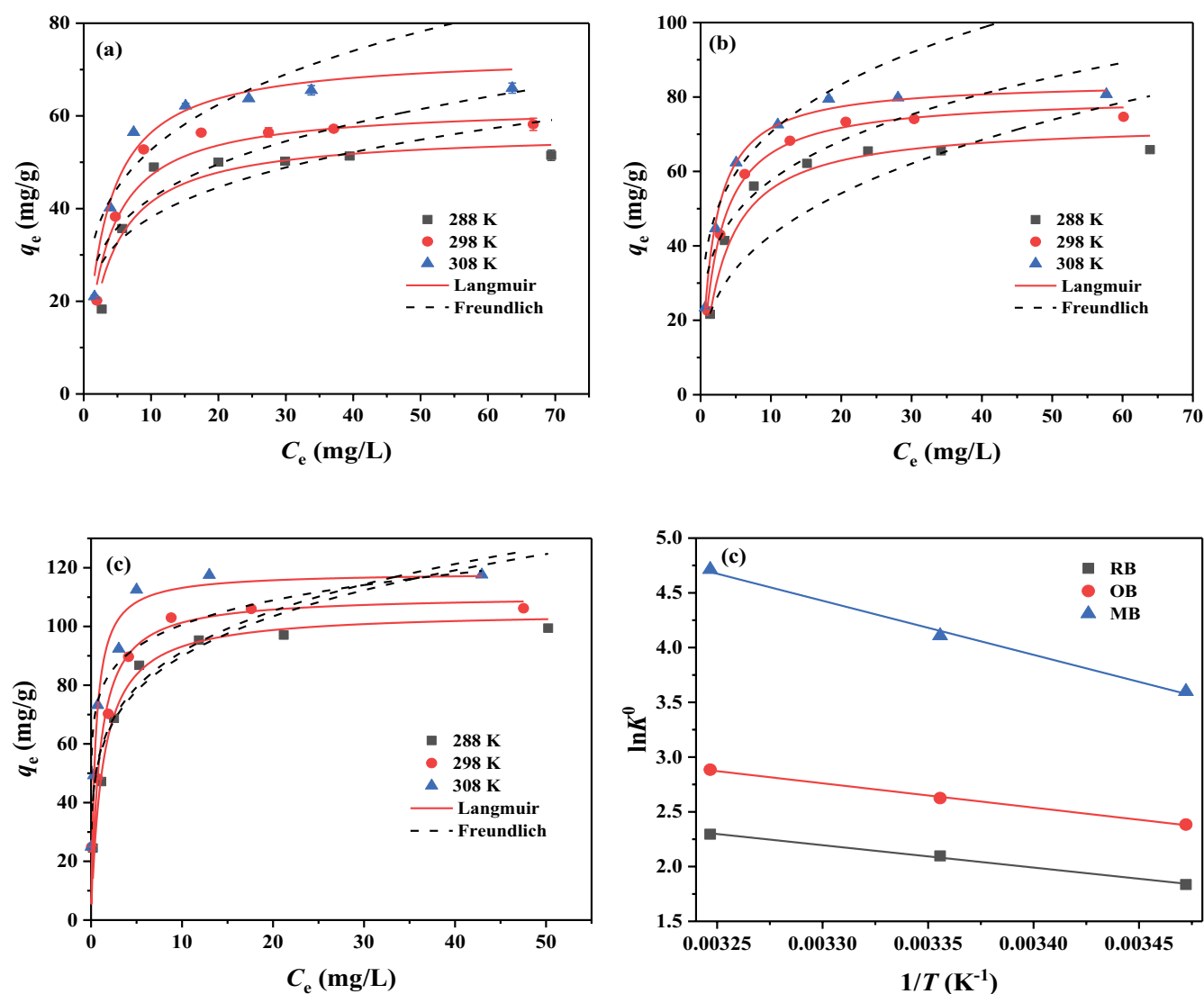


Fig. 4. Fitted isothermal model of adsorption for RB (a), OB (b), and MB (c). Adsorption thermodynamics of Ni(II) removal by the adsorbent.

Table 2
Fitting parameters of adsorption isothermal model

	T/K	Langmuir			Freundlich		
		q_{\max}	K_b	R_1^2	K_f	n	R_2^2
RB	288	56.58	0.272	0.923	22.64	4.420	0.748
	298	62.20	0.314	0.969	24.62	4.276	0.823
	308	73.33	0.333	0.953	29.96	4.079	0.780
OB	288	73.13	0.308	0.991	19.60	2.949	0.884
	298	80.25	0.421	0.997	32.81	4.095	0.777
	308	84.23	0.568	0.999	40.37	4.132	0.833
MB	288	105.11	0.779	0.983	56.26	4.917	0.874
	298	110.60	1.091	0.949	57.13	4.902	0.917
	308	118.45	2.131	0.965	77.21	8.706	0.911

The q_{\max} values of Ni(II) for different types of biochar are listed in Table 3. The q_{\max} of Ni(II) for different raw material biochar vary greatly [8,24,33,36]. In this study, the q_{\max} of MB were greater than those of biochar, indicating that MB had great potential to become a powerful adsorbent. To determine the cations in the adsorbent to provide adsorption sites for Ni(II) removal by ion-exchange, this was verified by measuring the changes in the concentrations of Na⁺ and Ca²⁺ in the solution after adsorption equilibrium at 298 K. The results were shown in Fig. S1. The concentrations of Na⁺ and Ca²⁺ in the solution gradually increased with the increase of the initial concentration of Ni(II). Notable, Ca²⁺ was released in higher amounts than Na⁺, which indicated that Ca²⁺ played a major role in the ion-exchange process. This phenomenon indicated that Na⁺ and Ca²⁺ provided adsorption sites for Ni(II) removal through ion-exchange [20].

3.4. Environmental factors

In general, pH played an important role in the adsorption process for the reason that it can affect the morphology of metal ions in solution as well as the electrical properties of the functional groups on the adsorbent surface. As shown in Fig. 5a, with the increase of the pH from 2.0 to 6.0,

the Ni(II) adsorption capacity on RB, OB, and MB reached a maximum value of 19.41, 22.30, and 24.18 mg/g, respectively. Then, with the increase of the initial pH of the solution to 10, the Ni(II) adsorption capacity on the adsorbent remained almost constant. At low pH, a large amount of H⁺ ions in the solution competed with Ni(II) for the active sites on the adsorbent surface, resulting in a lower adsorption amount at lower pH. It had also been suggested that a large amount of H⁺ occupies the O-containing functional groups on the adsorbent surface, causing the oxygen-containing functional groups on the adsorbent surface to be positively charged and generate electrostatic repulsion with the positively charged Ni(II) resulting in a lower adsorption capacity [29]. As the initial pH of the solution increased, the H⁺ in the solution decreased, which caused the adsorption to increase. As shown in Fig. 5b, the equilibrium solution pH was higher than the initial pH. When the solution pH was higher than 6.0, the equilibrium solution pH was alkaline. Previous research was shown that biochar had a strong pH buffering capacity and was able to buffer a weakly acidic solution to weak alkalinity, which led to the precipitation of heavy metal ions [37]. From the above analysis, co-precipitation and electrostatic interaction were identified as one of the mechanisms of Ni(II) removal by biochar.

The effects of coexisting ions such as Ca²⁺, Na⁺, Fe³⁺, Pb²⁺, and Cd²⁺ at different concentrations on the Ni(II) adsorption were investigated, as shown in Fig. 5c. After adjusting the pH of the solution to 6, 20 mg adsorbent was added to 10 mg/L Ni(II)-containing solution and reacted for 600 min. The effect of coexisting ions on the removal of Ni(II) is shown in Fig. 6c. The presence of Ca²⁺, Na⁺, and Fe³⁺ had almost no effect on the adsorption. However, a decrease in the adsorption efficiency was observed for both Pb²⁺ and Cd²⁺ concentrations from 0 to 50 mg/L. Among them, the presence of Pb²⁺ had a significant effect on the adsorption effect, followed by Cd²⁺ [19]. It was speculated that Ni(II) coexists with these two heavy metal ions in solution, thus competing with Ni(II) for adsorption [38,39]. The literature suggested that biochar had a lower affinity for Na⁺, Ca²⁺ and Fe³⁺ than Ni²⁺, and these cations had little effect on the Ni²⁺ removal by biochar [28]. A number of studies had shown that biochar preferentially adsorbs Cd²⁺ and Pb²⁺

Table 3
Comparison of the adsorption capacity of different biochar for Ni(II)

Adsorbents	Pyrolysis temperature	Experimental conditions	q_{\max}	References
Lotus stalks biochar	300	pH = 6.0, 298 K	6.4	[8]
	350	pH = 6.0, 298 K	10.3	[8]
	400	pH = 6.0, 298 K	10.5	[8]
Willow wood biochar	550	pH = 6.18, 298 K	9.80	[33]
Cattle manure biochar	550	pH = 6.18, 298 K	11.10	[33]
Sewage sludge biochar	500	pH = 7.0, 298 K	20.38	[24]
Sewage sludge biochar supported α -Fe ₂ O ₃ and α -FeOOH	500	pH = 7.0, 298 K	35.50	[24]
Magnetic biochar supported Mg-Fe hydrotalcite	600	pH = 5.5, 298 K	43.29	[36]
RB	500	pH = 6.0, 298 K	62.20	This work
OB	500	pH = 6.0, 298 K	80.25	This work
MB	500	pH = 6.0, 298 K	110.60	This work

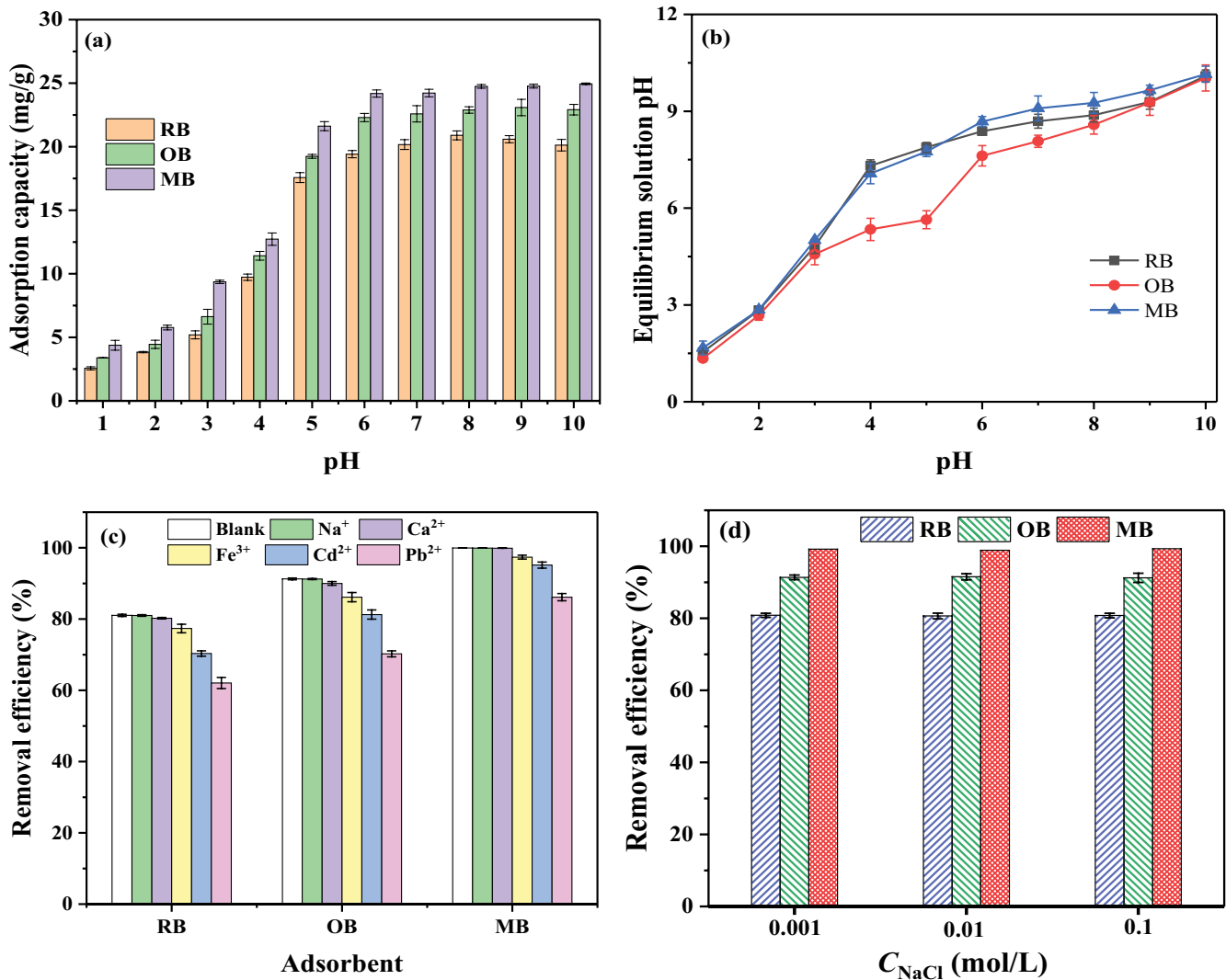


Fig. 5. Effect of solution pH on the Ni(II) adsorption (a) and the solution pH after adsorption equilibrium (b). Effect of co-existing ions (c) and background ions (d) on the Ni(II) removal.

in solution, which was attributed to the higher affinity of Cd²⁺ and Pb²⁺ for the O-containing functional groups on the biochar [10,38–40]. In addition, the competitive ability intensified with increasing concentration of coexisting ions, making the Ni(II) removal significantly inhibited.

The ionic strength effect of the background ion on the Ni(II) adsorption by the adsorbent was investigated under the conditions of 20 mg dosage, adsorption time 600 min, 10 mg/L of Ni(II), initial pH of 6.0 and 298 K. As shown in Fig. 5d, the increase in the ionic strength of NaCl from 0.001 to 0.1 mol/L had almost no effect on the Ni(II) removal by the adsorbent. This result suggested that the Ni(II) removal on the biochar was consistent with specific chemisorption, rather than specific physical adsorption [35]. In addition, previous literature had also been suggested that the removal process species was not affected by the background ion concentration, indicating that the removal process occurred inside the pore channel of the adsorbent and that a stronger inner layer complex was formed between Ni(II) and the biochars [10].

3.5. Adsorption mechanism

As shown in Fig. 6a, FTIR analysis of before and after Ni(II) adsorption was performed to determine the functional group changes of the adsorbent. Before the Ni(II) adsorption, RB had a strong and broad –OH diffraction peak at 3,401 cm⁻¹ [9,20,41]. The diffraction peak of –OH groups appeared enhanced and shifted after oxidation and Fe-impregnation, which indicated that oxidation and Fe-impregnation effectively enhanced the amount of O-containing functional groups in biochar. Previous literature reported that the number of O-containing functional groups in biochar increased and effectively enhanced the adsorption capacity of biochar for Cd²⁺ after H₂O₂ treatment [5,25,26]. In the RB, the vibrational peaks with a wavenumber of 1,623 and 1,428 cm⁻¹ were identified as C=O and C=O/C=C functional groups, respectively [14,15,42]. After modification, the intensity of the C=O and C=O/C=C diffraction peaks appeared enhanced or shifted, suggesting that oxidation and Fe-impregnation effectively increased

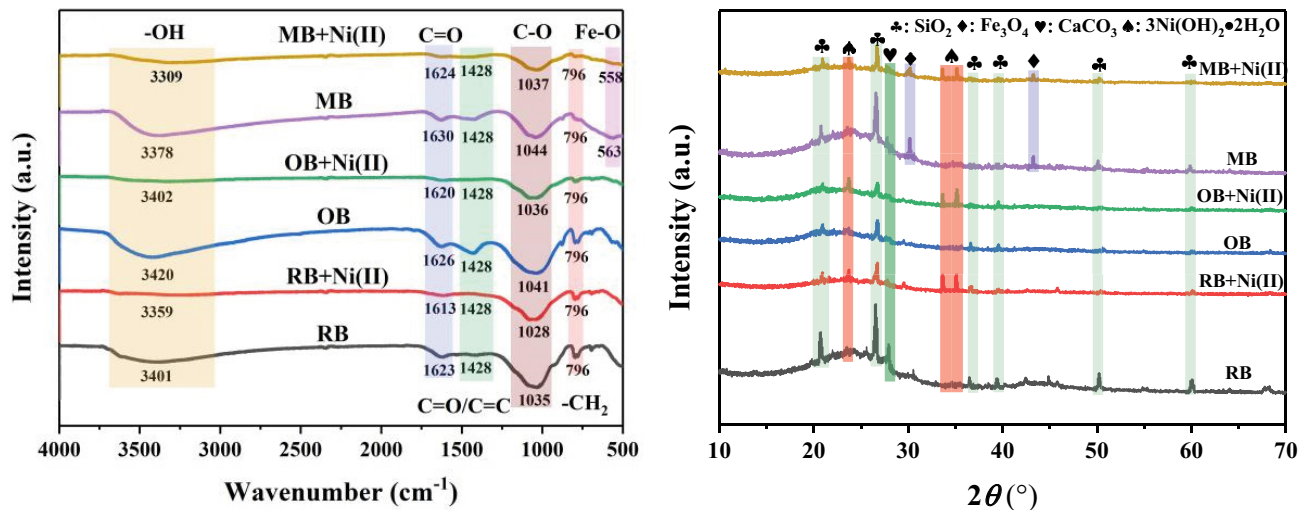


Fig. 6. FTIR and XRD of adsorbent before and after Ni(II) adsorption.

the content of O-containing functional groups in the biochar [25]. This was also consistent with previous studies reported. In addition, the vibrational peak at 1,035 cm⁻¹ was considered to be the C–O functional group [7,10]. After modification, the C–O groups showed a shift or intensity change, which was presumed to be due to oxidation and Fe-impregnation. In RB, a vibrational peak of unsaturated-CH₂ appears at 796 cm⁻¹ [30]. Likewise, the vibrational peak of unsaturated-CH₂ appears in the FTIR patterns of OB and MB. Notable, a vibrational peak at 563 cm⁻¹ appeared in MB, which was considered to be caused by the Fe–O group, which also indicated the successful introduction of iron oxides in the biochar after impregnation [26].

After Ni(II) adsorption, the broad and large –OH vibrational peak appeared to be weakened and shifted. In addition, the C=O group also appeared to be shifted and attenuated. Though the phenomenon indicated that the –OH and C=O groups in biochar were involved in the adsorption of Ni(II), and this result had been reported by many researchers [6,12,30]. Then, the weakening of the C=O/C=C group also occurred, which was presumed to be caused by the reaction of the group with Ni(II). Notable, the same phenomenon occurred with the C–O group, which suggested that this group was also involved in the removal of Ni(II) [24,31,32]. It has been reported that the removal of heavy metals from aqueous solutions by biochar was mainly due to its richness in O-containing functional groups that formed complexes with heavy metals, thus removing them from aqueous solutions [32]. This also confirmed that the O-containing functional groups in the three adsorbents were able to complex with Ni(II) in an aqueous solution to achieve the removal of Ni(II). Notable, the Fe–O group at 563 cm⁻¹ in MB shifted to 558 cm⁻¹ after adsorption and the peak intensity appeared to be weakened, which also indicated that the Fe–O group reacted with Ni(II) [24].

The XRD analysis before and after the Ni(II) adsorption by the adsorbent is shown in Fig. 6b. In RB, the main diffraction peaks were SiO₂ and CaCO₃, which indicated that RB contained certain inorganic substances. After

oxidation, the crystalline surfaces of SiO₂ and CaCO₃ appeared to weaken or disappear, which indicated that oxidation can remove the inorganic components from the biochar [37]. After Fe-impregnation, there were obvious diffraction peaks at 2θ of 30.25° and 43.20°, corresponding to Fe₃O₄ diffraction crystal plane, which indicated that the small particulate matter on the MB surface was Fe₃O₄ [24,26]. After adsorption, the SiO₂ crystal plane in the adsorbent appeared to weaken, while the CaCO₃ diffraction peaks disappeared or weakened, presumably because the CaCO₃ in the adsorbent dissolved in the solution. There were obvious diffraction peaks at 2θ of 23.80°, 33.74°, and 35.25°, and these peaks were identified as Ni(OH)₂·2H₂O precipitation according to the standard calorimetric comparison (JCS-PSD#22-0444), which indicated that precipitation reaction occurred during the adsorption process [36]. It had been shown by many scholars that biochar has a strong pH buffering ability to buffer weakly acidic solutions to alkaline, causing precipitation reactions of heavy metal ions in solution [36,37].

3.6. Removal of Ni(II) from actual water bodies

To judge whether the biochars can be practically applied, its Ni(II) removal effect needs to be tested in actual water. The Ni(II) removal on biochar was tested in three actual water bodies: deionized water (DW), tap water (TW), and Fu river water (RW, Chengdu, Sichuan Province, China). To compare the performance of the materials in different water bodies, the concentration of Ni(II) in the three water bodies was adjusted to 10 mg/L and the dosage of adsorbent was 20 mg. As shown in Fig. 7a, the experimental results showed that the removal efficiency of RB was 81% (DW), 76% (TW), and 65% (RW) after removing Ni(II) from the three water bodies for 600 min, respectively. Moreover, the removal efficiency of OB was 90% (DW), 83% (TW), and 78% (RW) for Ni(II) removal in different water bodies after 600 min, respectively. Notable, the Ni(II) removal efficiency in different water bodies by

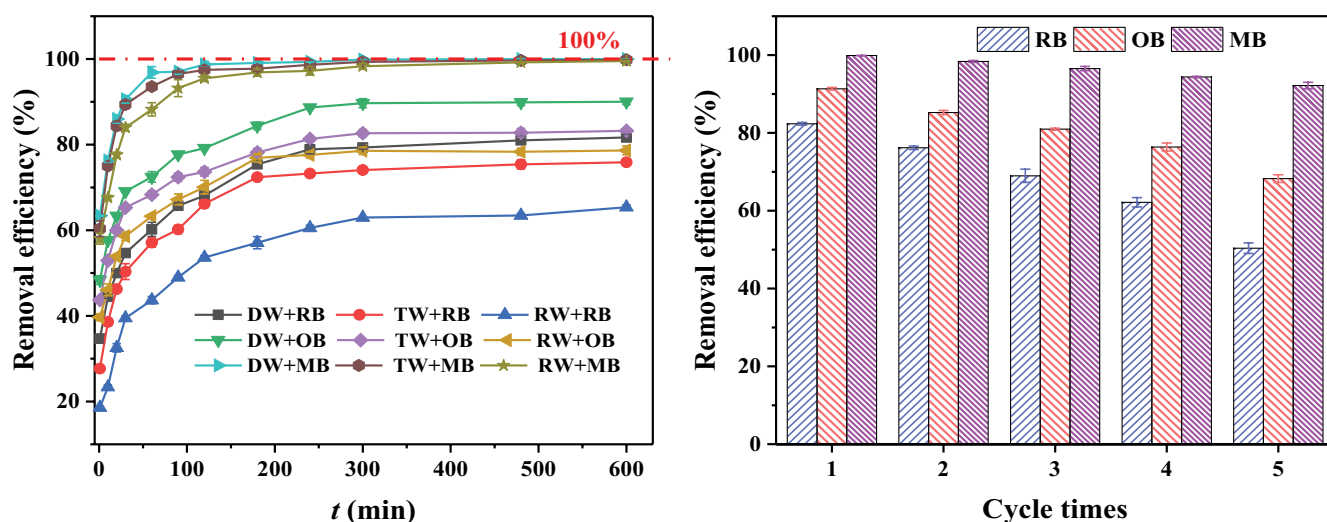


Fig. 7. Effect of different water bodies on Ni(II) removal by adsorbent (a) and adsorption-desorption experiment of Ni(II) by adsorbent (b).

MB was almost 100%, which indicated that MB was more effective in removing Ni(II) from the actual water bodies than RB and OB.

3.7. Adsorption-desorption experiments

The adsorption-desorption experiments were one of the key factors to evaluate the feasibility of an adsorbent and were performed for three adsorbents. In this experiment, 1 mol/L NaOH solution was used as the desorption solution, and desorption was performed by shaking at 150 rpm for 12 h at 298 K in a shaker. As shown in Fig. 7b, the Ni(II) removal efficiency on the three biochars gradually decreased with the repetitive experiments. After 5 adsorption-desorption experiments, the Ni(II) removal efficiency on RB, OB, and MB was 50%, 68%, and 91%, respectively. It was assumed that the decrease of Ni(II) removal was caused by the loss of adsorbent itself, the reduction of functional groups, and the clogging of pore channels. This result indicated that MB had excellent repeatability and practical value.

4. Conclusion

Different types of biochar adsorbents were prepared by oxidation and Fe-impregnation and used with the removal of Ni(II)-containing wastewater. The Ni(II) removal process by the adsorbents was following the Langmuir model and the pseudo-second-order model, indicating that the removal process was monolayer and homogeneous chemisorption. The theoretical maximum adsorption of Ni(II) by RB, OB, and MB was 62.20, 80.25, and 110.60 mg/g at 298 K, respectively. The Ni(II) removal efficiency on RB, OB, and MB was reached 80%, 91%, and 99% in the pH range of 5–10, respectively. The coexisting ions Na⁺, Ca²⁺, and Fe³⁺ had little effect on Ni(II) removal by biochar, while Cd²⁺ and Pb²⁺ had an inhibitory effect on Ni(II) removal. In different water bodies, the removal efficiency of Ni(II) by MB still reached 100%. After 5 adsorption-desorption experiments, the Ni(II) removal efficiency on RB, OB, and

MB remained around 51%, 70%, and 90%, respectively. Notable, co-precipitation, ion-exchange, electrostatic interaction, and complexation may exist in the mechanism of Ni(II) removal by biochar. This study suggested that Fe-impregnated biochar had the potential and prospect for better treatment of Ni(II)-containing wastewater generated from alloy manufacturing.

Supplementary materials

Table S1. Parameters fitted to the intraparticle diffusion model. Table S2. Thermodynamic fitting parameters. Fig. S1. The release of cations from the solution at 298 K.

Funding

This work was supported by National Key R&D Program (2018YFC1505404) and Sichuan Provincial Science and Technology Department Science and Technology Plan Project (No.2021YJ0033).

Conflicts of interest

The authors declare that they have no competing financial interests.

References

- [1] A. El-Naggar, N. Ahmed, A.A. Mosa, N.K. Niazi, B. Yousaf, A. Sharma, B. Sarkar, Y. Cai, S.X. Chang, Nickel in soil and water: sources, biogeochemistry, and remediation using biochar, *J. Hazard. Mater.*, 419 (2021) 126421, doi: 10.1016/j.jhazmat.2021.126421.
- [2] Md.S. Alam, D. Gorman-Lewis, C. Ning, S.L. Flynn, S.O. Yong, K.O. Konhauser, D.S. Alessi, Thermodynamic analysis of nickel(II) and zinc(II) adsorption to biochar, *Environ. Sci. Technol.*, 52 (2018) 6246–6255.
- [3] Z. Shen, Y. Zhang, O. McMillan, F. Jin, A. Al-Tabbaa, Characteristics and mechanisms of nickel adsorption on biochars produced from wheat straw pellets and rice husk, *Environ. Sci. Pollut. Res.*, 24 (2017) 12809–12819.

- [4] E. Singh, A. Kumar, R. Mishra, S. You, L. Singh, S. Kumar, R. Kumar, Pyrolysis of waste biomass and plastics for production of biochar and its use for removal of heavy metals from aqueous solution, *Bioresour. Technol.*, 320 (2020) 124278, doi: 10.1016/j.biortech.2020.124278.
- [5] G.D. Sheng, C.C. Huang, G.H. Chen, S. Jiang, X.M. Ren, B.W. Hu, J.Y. Ma, X.K. Wang, Y.Y. Huang, A. Alsaedi, T. Hayat, Adsorption and co-adsorption of graphene oxide and Ni(II) on iron oxides: a spectroscopic and microscopic investigation, *Environ. Pollut.*, 233 (2018) 125–131.
- [6] R.-N. Mourgela, P. Regkouzas, F.-M. Pelleri, E. Diamadopoulos, Ni(II) adsorption on biochars produced from different types of biomass, *Water Air Soil Pollut.*, 231 (2020) 1–16, doi: 10.1007/s11270-020-04591-1.
- [7] Z. Mahdi, A.E. Hanandeh, Q.J. Yu, Electro-assisted adsorption of heavy metals from aqueous solutions by biochar, *Water Sci. Technol.*, 81 (2020) 801–812.
- [8] H. Liu, S. Liang, J.H. Gao, H.H. Ngo, W.S. Guo, Z.Z. Guo, Y.R. Li, Development of biochars from pyrolysis of lotus stalks for Ni(II) sorption: Using zinc borate as flame retardant, *J. Anal. Appl. Pyrolysis*, 107 (2014) 336–341.
- [9] A. El Hanandeh, Z. Mahdi, M.S. Imtiaz, Modelling of the adsorption of Pb, Cu and Ni ions from single and multi-component aqueous solutions by date seed derived biochar: comparison of six machine learning approaches, *Environ. Res.*, 192 (2021) 110338, doi: 10.1016/j.envres.2020.110338.
- [10] N. Esfandiar, R. Suri, E.R. McKenzie, Competitive sorption of Cd, Cr, Cu, Ni, Pb and Zn from stormwater runoff by five low-cost sorbents; effects of co-contaminants, humic acid, salinity and pH, *J. Hazard. Mater.*, 423 (2021) 126938, doi: 10.1016/j.jhazmat.2021.126938.
- [11] L.J. Dong, W.S. Linghu, D.L. Zhao, Y.Y. Mou, B.W. Hu, A.M. Asiri, K.A. Alamry, D. Xu, J. Wang, Performance of biochar derived from rice straw for removal of Ni(II) in batch experiments, *Water Sci. Technol.*, 2017 (2018) 824–834.
- [12] M.T. Amin, A.A. Alazba, M. Shafiq, Comparative sorption of nickel from an aqueous solution using biochar derived from banana and orange peel using a batch system: kinetic and isotherm models, *Arabian J. Sci. Eng.*, 44 (2019) 10105–10116.
- [13] S.J. Yu, H.W. Pang, S.Y. Huang, H. Tang, S.Q. Wang, M.Q. Qiu, Z.S. Chen, H. Yang, G. Song, D. Fu, B.W. Hu, X.X. Wang, Recent advances in metal-organic framework membranes for water treatment: a review, *Sci. Total Environ.*, 800 (2021) 149662, doi: 10.1016/j.scitotenv.2021.149662.
- [14] U. Ali, M. Shaaban, S. Bashir, R.L. Gao, Q.L. Fu, J. Zhu, H.Q. Hu, Rice straw, biochar and calcite incorporation enhance nickel (Ni) immobilization in contaminated soil and Ni removal capacity, *Chemosphere*, 244 (2020) 125418, doi: 10.1016/j.chemosphere.2019.125418.
- [15] S. Biswas, B.C. Meikap, T.K. Sen, Adsorptive removal of aqueous phase copper (Cu²⁺) and nickel (Ni²⁺) metal ions by synthesized biochar-biopolymeric hybrid adsorbents and process optimization by response surface methodology (RSM), *Water Air Soil Pollut.*, 230 (2019) 197–220.
- [16] X.L. Hu, Y.W. Xue, L.N. Liu, Y.F. Zeng, L. Long, Preparation and characterization of Na₂S-modified biochar for nickel removal, *Environ. Sci. Pollut. Res.*, 25 (2018) 9887–9895.
- [17] L.P. Liang, F.F. Xi, W.S. Tan, X. Meng, B.W. Hu, X.K. Wang, Review of organic and inorganic pollutants removal by biochar and biochar-based composites, *Biochar*, 3 (2021) 255–281.
- [18] M.Q. Qiu, B.W. Hu, Z.S. Chen, H. Yang, L. Zhuang, X.K. Wang, Challenges of organic pollutant photocatalysis by biochar based catalysts, *Biochar*, 3 (2021) 117–123.
- [19] A.D. Zand, M.R. Abyaneh, Equilibrium and kinetic studies in remediation of heavy metals in landfill leachate using wood-derived biochar, *Desal. Water Treat.*, 141 (2019) 279–300.
- [20] Z. Mahdi, Q.J. Yu, A.E. Hanandeh, Investigation of the kinetics and mechanisms of nickel and copper ions adsorption from aqueous solutions by date seed derived biochar, *J. Environ. Chem. Eng.*, 6 (2018) 1171–1181.
- [21] S. Zhang, J.Q. Wang, Y. Zhang, J.Z. Ma, L.T.Y. Huang, S.J. Yu, L. Chen, G. Song, M.Q. Qiu, X.X. Wang, Applications of water-stable metal-organic frameworks in the removal of water pollutants: a review, *Environ. Pollut.*, 291 (2021) 118076, doi: 10.1016/j.envpol.2021.118076.
- [22] R. Wahid, N.F.Q. Zuhaidi, Y. Yusof, J. Jamel, D. Kanakaraju, Z. Ngaini, Chemically treated microwave-derived biochar: an overview, *Biomass Bioenergy*, 107 (2017) 411–421.
- [23] J. Zhang, N. Zhang, F.M.G. Tack, S. Sato, D.S. Alessi, P. Oleszczuk, H. Wang, X. Wang, S.S. Wang, Modification of ordered mesoporous carbon for removal of environmental contaminants from aqueous phase: a review, *J. Hazard. Mater.*, 418 (2021) 126266, doi: 10.1016/j.jhazmat.2021.126266.
- [24] L. Yang, L.Y. He, J.M. Xue, L. Wu, Z.L. Zhang, Highly efficient nickel(II) removal by sewage sludge biochar supported α -Fe₂O₃ and α -FeOOH: sorption characteristics and mechanisms, *PLoS One*, 14 (2019) e0218114, doi: 10.1371/journal.pone.0218114.
- [25] R.H. Chang, S.P. Sohi, F.Q. Jing, Y.Y. Liu, J.W. Chen, A comparative study on biochar properties and Cd adsorption behavior under effects of ageing processes of leaching, acidification and oxidation, *Environ. Pollut.*, 254 (2020) 113123, doi: 10.1016/j.envpol.2019.113123.
- [26] J. Iftikhar, J. Wang, Q.L. Wang, T. Wang, H.B. Wang, A. Khan, A. Jawad, T.T. Sun, X. Jiao, Z.Q. Chen, Highly efficient lead distribution by magnetic sewage sludge biochar: sorption mechanisms and bench applications, *Bioresour. Technol.*, 238 (2017) 399–406.
- [27] W.J. Yin, W. Zhang, C.C. Zhao, J.T. Xu, Evaluation of removal efficiency of Ni(II) and 2,4-DCP using in situ nitrogen-doped biochar modified with aquatic animal waste, *ACS Omega*, 4 (2019) 19366–19374.
- [28] H.H. Lyu, B. Gao, F. He, A.R. Zimmerman, C. Ding, H. Huang, J.C. Tang, Effects of ball milling on the physicochemical and sorptive properties of biochar: experimental observations and governing mechanisms, *Environ. Pollut.*, 233 (2018) 54–63.
- [29] A.A. Mosa, A. El-Ghamry, H. Al-Zahrani, E.M. Selim, A. El-Khateeb, Chemically modified biochar derived from cotton stalks: characterization and assessing its potential for heavy metals removal from wastewater, *Environ. Biodiv. Soil Security*, 1 (2017) 33–45.
- [30] S. Vilvanathan, S. Shanthakumar, Ni²⁺ and Co²⁺ adsorption using *Tectona grandis* biochar: kinetics, equilibrium and desorption studies, *Environ. Technol.*, 39 (2017) 464–478.
- [31] S.Y. Wang, Y.K. Tang, K. Li, Y.Y. Mo, H.F. Li, Z.Q. Gu, Combined performance of biochar sorption and magnetic separation processes for treatment of chromium-contained electroplating wastewater, *Bioresour. Technol.*, 174 (2014) 67–73.
- [32] Q.W. Wu, L. Meng, Z.H. Zhang, Q.S. Luo, Adsorption behaviors of Ni²⁺ onto reed straw biochar in the aquatic solutions, *Environ. Chem.*, 34 (2015) 1703–1709.
- [33] S. Wang, J.-H. Kwak, M.S. Islam, M.A. Naeth, S.X. Chang, Biochar surface complexation and Ni(II), Cu(II), and Cd(II) adsorption in aqueous solutions depend on feedstock type, *Sci. Total Environ.*, 712 (2020) 136538, doi: 10.1016/j.scitotenv.2020.136538.
- [34] J.J. Xia, L. Yuan, S.T. Tong, Adsorption of Ni²⁺ and Cu²⁺ on modified biochar, *Environ. Prot. Chem. Ind.*, 36 (2016) 428–433.
- [35] Y. Zhao, Y.L. Li, D. Fan, J.P. Song, F. Yang, Application of kernel extreme learning machine and kriging model in prediction of heavy metals removal by biochar, *Bioresour. Technol.*, 329 (2021) 124876, doi: 10.1016/j.biortech.2021.124876.
- [36] J.G. Fu, Y. Jia, Z. Li, Y.T. Huang, Preparation of Mg-Fe hydroxalite supported on magnetic biochar and its adsorption capacity to Cd(II) and Ni(II) from water, *Environ. Prot. Chem. Ind.*, 39 (2019) 574–580.
- [37] T. Chen, Z.Y. Zhou, H. Rong, R.H. Meng, H.T. Wang, W.J. Lu, Adsorption of cadmium by biochar derived from municipal sewage sludge: impact factors and adsorption mechanism, *Chemosphere*, 134 (2015) 286–293.
- [38] C.S. Wang, M.X. He, F. Zhou, L. Chen, J.Z. Zhu, Heavy metal ion adsorption properties and stability of amine-sulfur modified biochar in aqueous solution, *Environ. Sci.*, 42 (2021) 874–882.
- [39] B.J. Ni, Q.S. Huang, C. Wang, T.Y. Ni, J. Sun, W. Wei, Competitive adsorption of heavy metals in aqueous solution onto biochar derived from anaerobically digested sludge, *Chemosphere*, 219 (2019) 351–357.

- [40] R. Shan, Y.Y. Shi, J. Gu, Y.Z. Wang, H.R. Yuan, Single and competitive adsorption affinity of heavy metals toward peanut shell-derived biochar and its mechanisms in aqueous systems, *Chin. J. Chem. Eng.*, 28 (2020) 1375–1383.
- [41] R.R. Liu, H. Wang, L. Han, B.W. Hu, M.Q. Qiu, Reductive and adsorptive elimination of U(VI) ions in aqueous solution by SFeS@Biochar composites, *Environ. Sci. Pollut. Res.*, 28 (2021) 55176–55185.
- [42] R.R. Liu, Y.H. Zhang, B.W. Hu, H. Wang, Improved Pb(II) removal in aqueous solution by sulfide@biochar and polysaccharose-FeS@biochar composites: efficiencies and mechanisms, *Chemosphere*, 287 (2022) 132087, doi: 10.1016/j.chemosphere.2021.132087.

Supplementary information

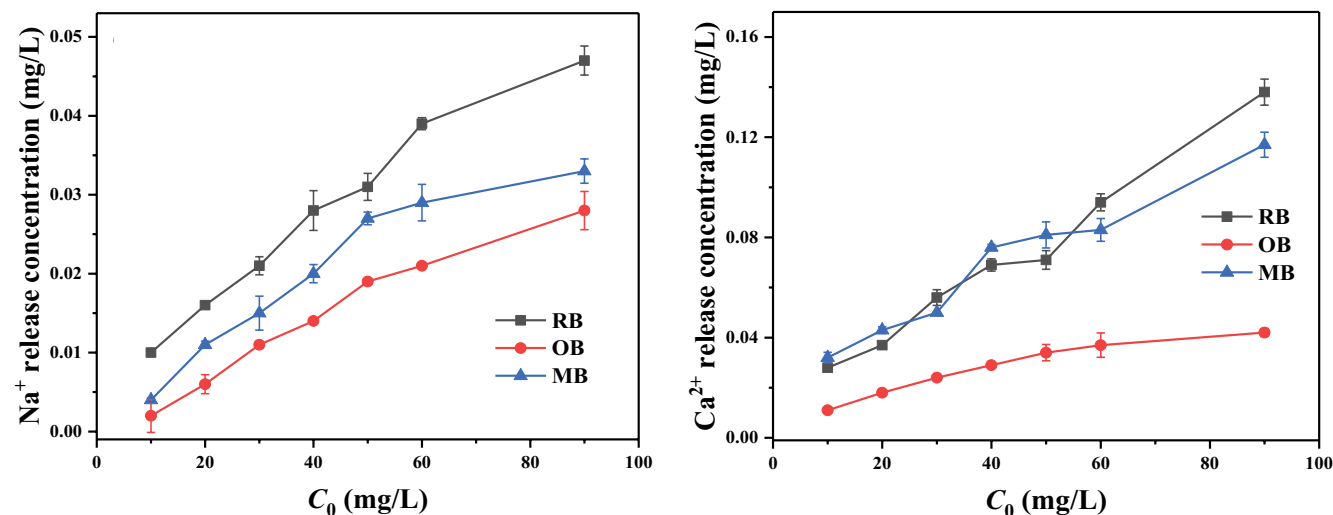


Fig. S1. The release of cations from the solution at 298 K.

Table S1
Parameters fitted to the intraparticle diffusion model

	Intraparticle diffusion model								
	Phase I			Phase II			Phase III		
	k_1	C_1	R_1^2	k_2	C_2	R_2^2	k_3	C_3	R_3^2
RB	1.950	6.75	0.997	0.917	8.65	0.991	0.153	17.52	0.960
OB	2.682	7.41	0.999	0.970	11.99	0.981	0.050	21.58	0.934
MB	1.195	16.42	0.841	0.051	23.88	0.474	0.032	24.47	0.837

Table S2
Thermodynamic fitting parameters

	T/K	ΔG° (kJ/mol)	ΔH° (kJ/mol)	ΔS° (kJ/mol)
RB	288	-4.40		
	298	-5.20	16.99	74.31
	308	-5.89		
OB	288	-5.71		
	298	-6.50	18.45	83.85
	308	-7.39		
MB	288	-8.62		
	298	-10.18	41.06	172.32
	308	-12.07		